

PAPER • OPEN ACCESS

Combined rings and horizontal steel pipe as hysteretic dampers

To cite this article: J Utomo *et al* 2019 *IOP Conf. Ser.: Mater. Sci. Eng.* **615** 012082

View the [article online](#) for updates and enhancements.

You may also like

- [Magnetorheological fluid dampers: a review of parametric modelling](#)
D H Wang and W H Liao
- [A new magnetorheological damper for seismic control](#)
Yang Ding, Lu Zhang, Hai-Tao Zhu et al.
- [A comparative work on vibration control of a quarter car suspension system with two different magneto-rheological dampers](#)
Jhin Ha Park, Wan Ho Kim, Cheol Soo Shin et al.



ECS
The
Electrochemical
Society
Advancing solid state &
electrochemical science & technology

DISCOVER
how sustainability
intersects with
electrochemistry & solid
state science research

Combined rings and horizontal steel pipe as hysteretic dampers

J Utomo^{*1,2}, M Moestopo², A Surahman² and D Kusumastuti²

¹Universitas Atma Jaya Yogyakarta, Yogyakarta, Indonesia

²Institut Teknologi Bandung, Bandung, Indonesia

*jun.utomo@gmail.com

Abstract. A new combined rings and horizontal steel pipe as hysteretic dampers for seismic resistant steel structures have been developed. Simulation studies for various models of the dampers have been carried out under cyclic shear loadings. In each model, different strengthening strategy applied to the combined rings and horizontal steel pipe damper was explored. The chosen model among simulated dampers experienced extensive yield under different cyclic loadings. The specimens of the chosen model have been tested using the same four different cyclic shear loadings, which are ultralow-cycle fatigue (ULCF) loads representing extreme earthquakes. At the end of each testing, all tested dampers experienced ductile fracture. The test results showed all dampers have a stable hysteretic response under ULCF loads. All dampers exhibit excellent ductility represented by many plastic cycles before failures. If enough number of dampers are installed in building structures, the combined rings and horizontal steel pipe dampers can be used as the seismic energy dissipating devices for steel structures.

1. Introduction

Two types of horizontal steel pipe dampers for bridges have been introduced by Mahjoubi and Maleki [1], namely dual and infilled pipe dampers. Recently a new combined rings and horizontal steel pipe damper for buildings has been developed. Ring and horizontal steel pipe as damper's components have similar characteristics: (1) both components are very ductile (their strength); (2) both components have moderate horizontal stiffness (their weakness). If both properties of the component are combined together, ring and horizontal steel pipe maintain their excellent ductility but increase their horizontal stiffness. Currently, seismic dampers are highly needed to cope with the increasing code-demand for buildings minimum based shear. The developed damper has been numerically studied and tested experimentally using four different cyclic shear loadings which represent ultralow-cycle fatigue (ULCF) loads. The ULCF loads are used to represent extreme earthquakes. The damper can be installed in steel structures using different configurations to absorb seismic strain energy and to reduce the lateral displacement at each floor level of the structures, therefore structural and nonstructural components in the structures are protected.

2. Ductile fracture simulation

Simulation studies were conducted using ABAQUS [2] to seek the potential model of the combined rings and horizontal steel pipe damper. Among the various models studied, the chosen model of the



damper is shown in figure 1. The dimensions of the model are as follows: (1) Ring has thickness $t = 16$ mm and width $w = 25$ mm, and (2) Schedule 80 steel pipe has diameter $D = 114.3$ mm, thickness $t = 8.6$ mm and length $l = 200$ mm. Sharp corners are rounded to avoid stress concentration.

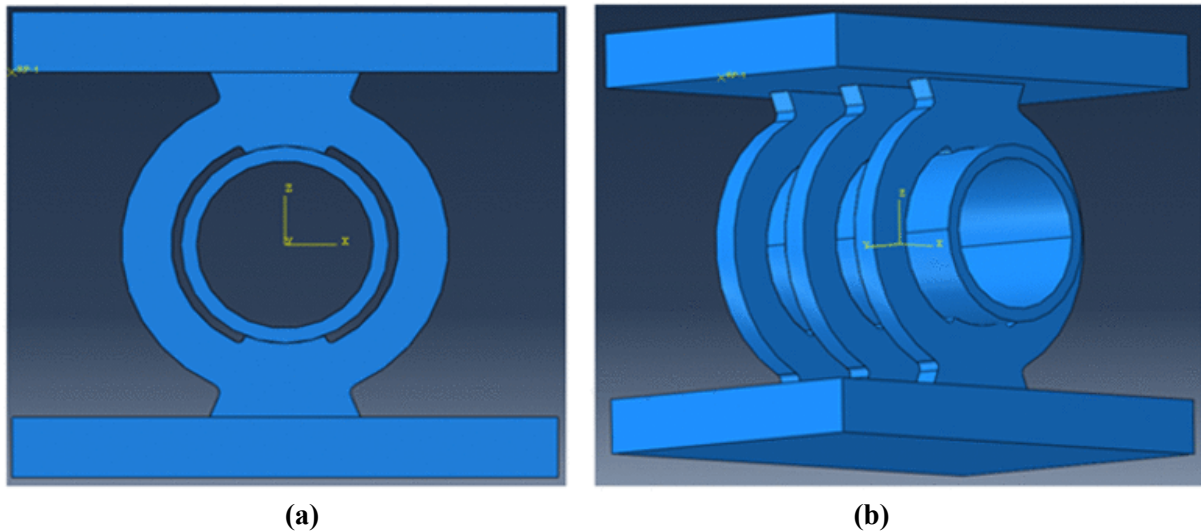


Figure 1. The final model of the damper: (a) Front view and (b) 3-D view.

Points of high intense stress can be identified by observing von Mises stress distribution of the damper under cyclic shear loadings. The strategies used to develop damper, von Mises stress distribution of the final model under increasing amplitude cyclic loading, and points of high intense stress, are shown in figure 2. Welded connections are placed in low stress areas so that the fractures in Heat Affected Zone (HAZ) areas were avoided. A small gap is provided between the pipe and the rings to avoid physical contact (interaction) between the pipe and the rings.

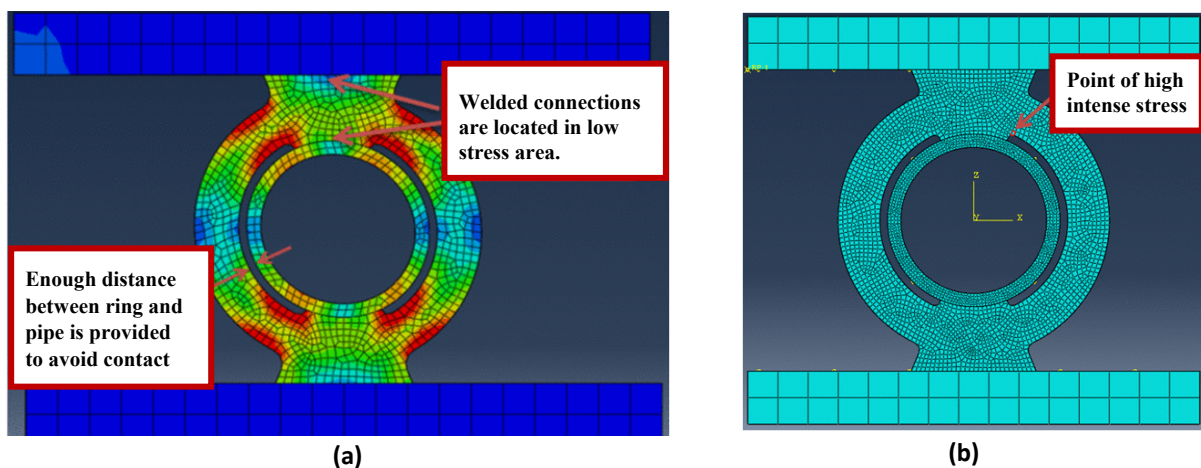


Figure 2. Combined rings and horizontal steel pipe damper under cyclic shear loadings: (a) Strategies for developing damper and von Mises stress distribution; (b) Point of high intense stress.

The damper is expected to be able to dissipate significant amount of strain energy through many plastic cycles. The number of plastic cycles under different ULCF loadings can be estimated from ductile fracture simulation. There are situations where the triaxial stress (*Triax*) at points of high intense stress are constant under different cyclic loadings. The well-known SMCS (Stress Modified

Critical Strain) model, which is derived based on constant triaxial stress ($Triax$), can be used to predict the onset of fractures in the damper under ULCF loadings.

The four ULCF loadings, used for ductile fracture simulation, are as follows:

- Cyclic shear loading following ATC-24 loading protocol.
- Cyclic shear loading with increasing amplitude of 2x yielding displacement (δ_y) at each step of loading ($\Phi=2$).
- Cyclic shear loading with increasing amplitude of 10x yielding displacement (δ_y) at each step loading ($\Phi=10$).
- Cyclic shear loading with constant amplitude of 30x yielding displacement (δ_y) at each step of loading ($\Delta=30$).

The stable simulated hysteretic curves due to four ULCF loads described above are shown in figure 3. Post processing was done to the results of the simulation studies to obtain the relationship of the triaxiality stress ($Triax$) and the plastic equivalent strain ($PEEQ$) due to four ULCF loads above (ATC-24, $\Phi=2$, $\Phi=10$ and $\Delta=30$). The four $Triax$ - $PEEQ$ relationship are shown in figure 4.

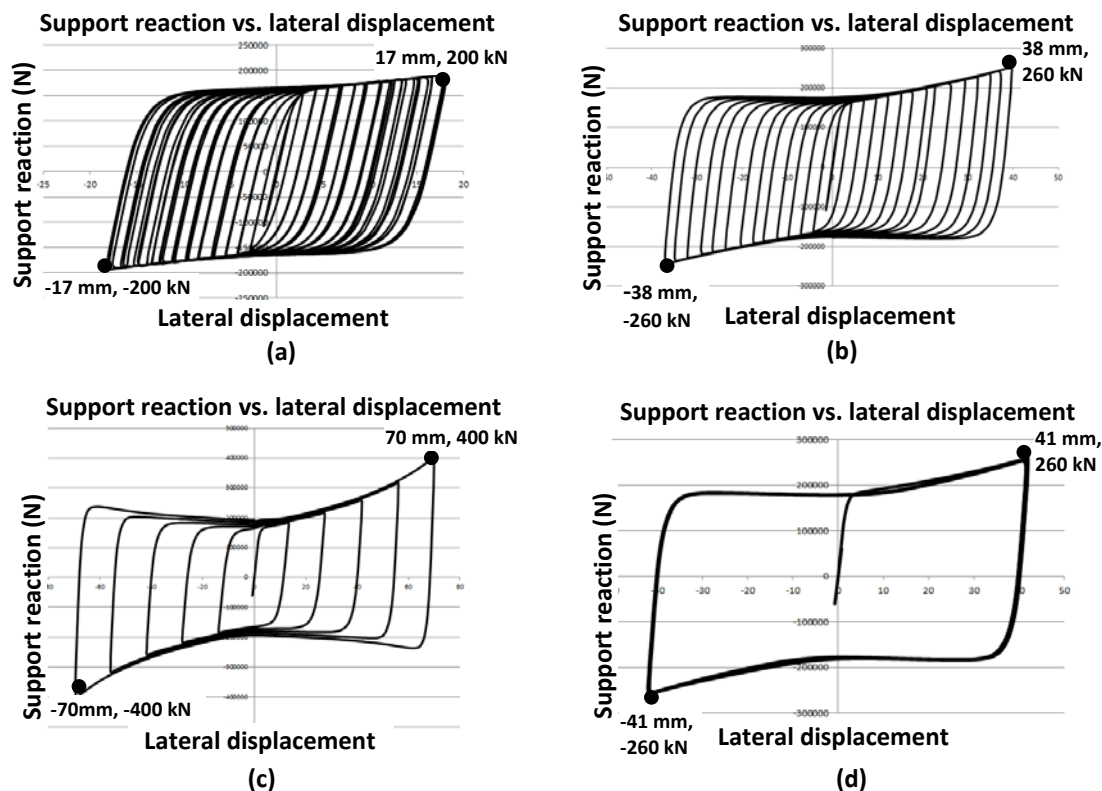


Figure 3. Stable simulated hysteretic curves due to four ULCF loadings: (a) ATC-24; (b) $\Phi=2$; (c) $\Phi=10$ and (d) $\Delta=30$.

As shown in figure 4, the triaxial stress ($Triax$) is relatively constant while the plastic strain equivalent ($PEEQ$) accumulates during a cyclic loading, therefore the loading history of the damper can be ignored. The SMCS (Stress Modified Critical Strain) model, which was derived based on constant triaxial stress, is used to calculate critical plastic strain $\epsilon_p^{critical}$. Ductile fracture prediction requires material toughness index α . Kanvinde and Deierlein [3] has done a lot of testing for various type of steels. The $\alpha=4.2$ closely matches the value of damper material. Ductile fracture prediction for ATC-24 loading protocol is conducted as follows: (1) triaxial stress ($Triax$) = 0.5, (2) critical plastic

strain $\varepsilon_p^{critical} = \alpha \cdot \exp(-1.5Triax) = 4.2 \exp(-1.5Triax) = 1.98$. During cyclic loadings, the absolute value of plastic strain equivalent (*PEEQ*) is accumulated. A good approximation for predicting the onset of ductile fracture uses $2 \times \varepsilon_p^{critical} = 2 \times 1.98 = 3.97$. Plot of the *PEEQ* vs. Pseudo time for ATC-24 loading is shown in figure 5. From figure 5, ductile fracture is predicted to happen at 155.96 second. Plotting the ATC-24 cyclic loading protocol, the number of cycle prediction is shown in figure 6. Counting the number of cycles in figure 6, ductile fracture is predicted to happen at 30th cycle. In a similar way, for three other ULCF loads ($\Phi=2$, $\Phi=10$, and $\Delta=30$), ductile fractures are predicted to happen at 13th, 6th and 5th cycle respectively.

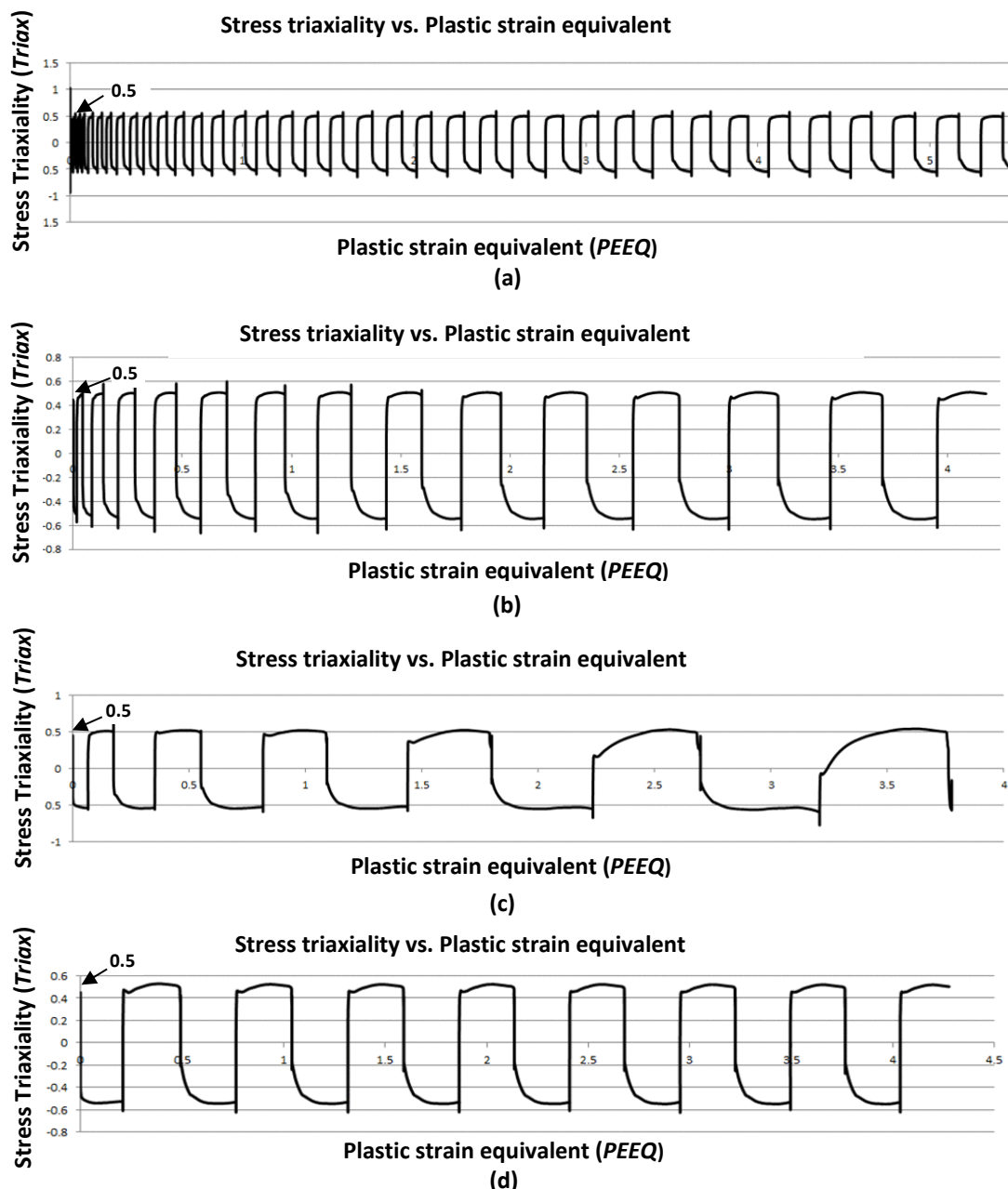


Figure 4. *Triax-PEEQ* relationship under four cyclic loadings: (a) ATC-24; (b) $\Phi=2$; (c) $\Phi=10$ and (d) $\Delta=30$.

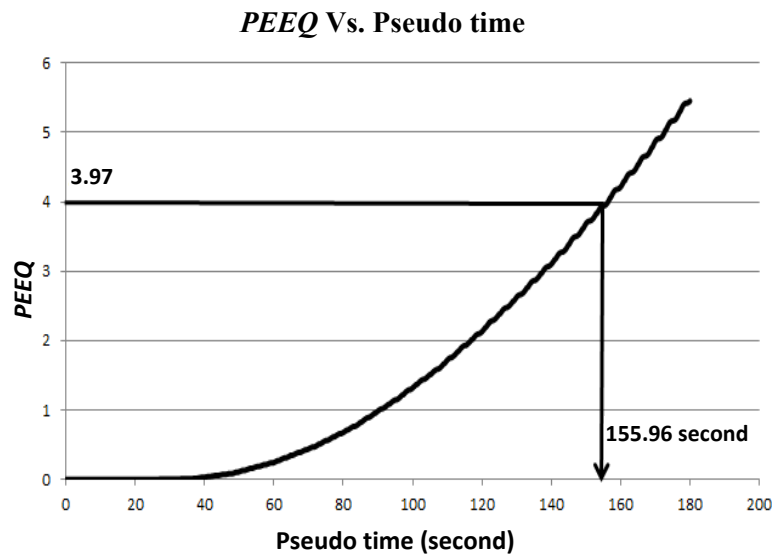


Figure 5. Ductile fracture prediction for ATC-24 loading protocol.

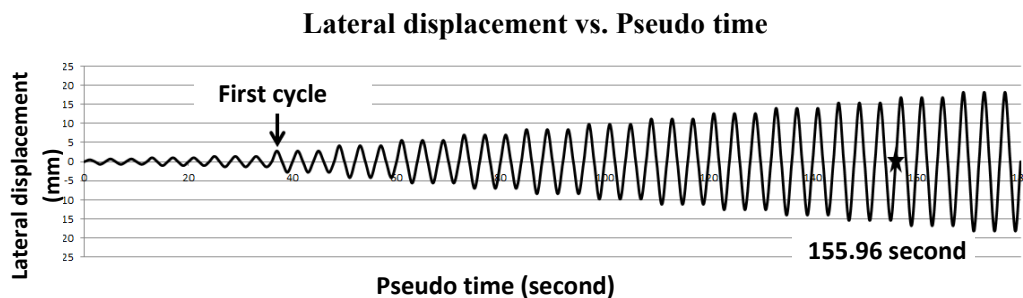


Figure 6. Ductile fracture prediction due to ATC-24 loading protocol.

3. Experimental testing

Extreme earthquakes are assumed to be represented by the four ULCF loadings described above. The ULCF loads were used for testing the specimens of the dampers. The setup specimen of the combined rings and horizontal steel pipe damper and the fracture specimen at the end of each test are shown in figure 7. The damper was fixed at the bottom and mounted on the bottom flange of the beam. The hydraulic actuator, which generates cyclic lateral displacements was mounted on the left side of the mounting beam. The end of each test was characterized by ductile fracture at the point of high intense stress (see bottom right at figure 7(b)). The point of high intense stress is shown in figure 2. From numerical simulation and experimental testing, the number of plastic cycles, when ductile fractures are happened, are shown in table 1. It can be seen from table 1 that the numerical simulation predicts the onset of ductile fractures well enough.

Table 1. First yield and number of plastic cycles at the onset of fractures.

ULCF Loading	δ_y (mm)	Number of Plastic Cycles (Numerical Simulation)	Number of Plastic Cycles (Experimental Testing)
ATC-24	1.77	30	31
$\Phi=2$	1.80	13	12
$\Phi=10$	1.80	6	6
$\Delta=30$	1.80	5	8



Figure 7. Setup specimen for combined rings and horizontal steel pipe damper: (a) Mounting beam for testing specimens and (b) Fracture at point of high intense stress in the tested specimen.

Four stable hysteretic curves of the tested specimens under four ULCF loadings are shown in figure 8. These hysteretic curves can be compared to the similar curves obtained from numerical simulation shown in figure 3. It should be noted that the hysteretic curves in figure 3 contain more plastic cycles than the ones after ductile fracture were predicted. The correct number of plastic cycles in figure 3 after ductile fracture simulation are 30, 13, 6 and 5 respectively.

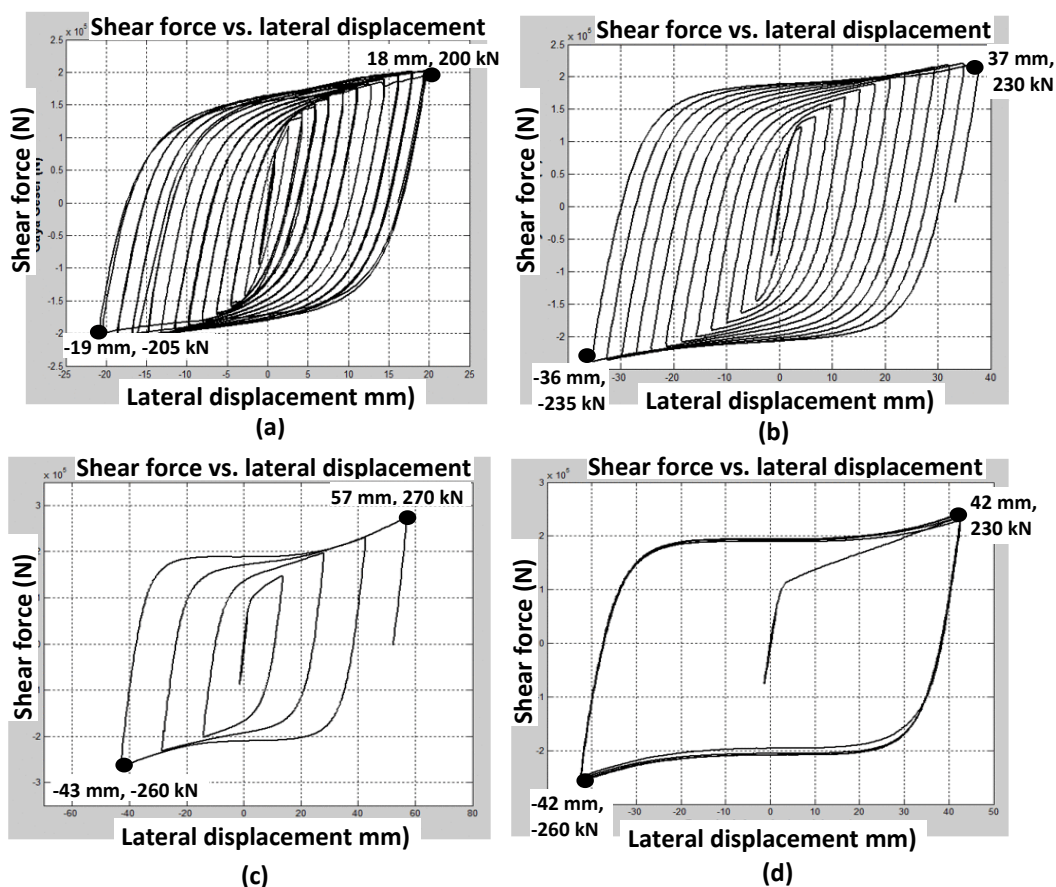


Figure 8. Stable hysteretic curves of the tested specimens under four ULCF loadings: (a) $ATC=24$; (b) $\Phi=2$; (c) $\Phi=10$ and (d) $\Delta=30$.

All hysteretic curves in figure 8 are stable and fat, indicating a good performance of the combined rings and horizontal steel pipe damper as a dissipating energy device.

4. Dissipated strain energy and accumulated plastic deformation

The dissipated strain energy and accumulated plastic deformation of the damper under ULCF loadings can be quantified by first decomposing the stable hysteretic curves in figure 8 into skeleton parts and Bauschinger parts following the procedures proposed by Benavent Climent [4]. The skeleton parts and Bauschinger parts due to ATC-24 and $\Phi=2$ ULCF loadings are shown in figure 9. The skeleton parts and Bauschinger parts due to $\Phi=10$ and $\Delta=30$ ULCF loadings, which can be obtained in a similar way, are not shown.

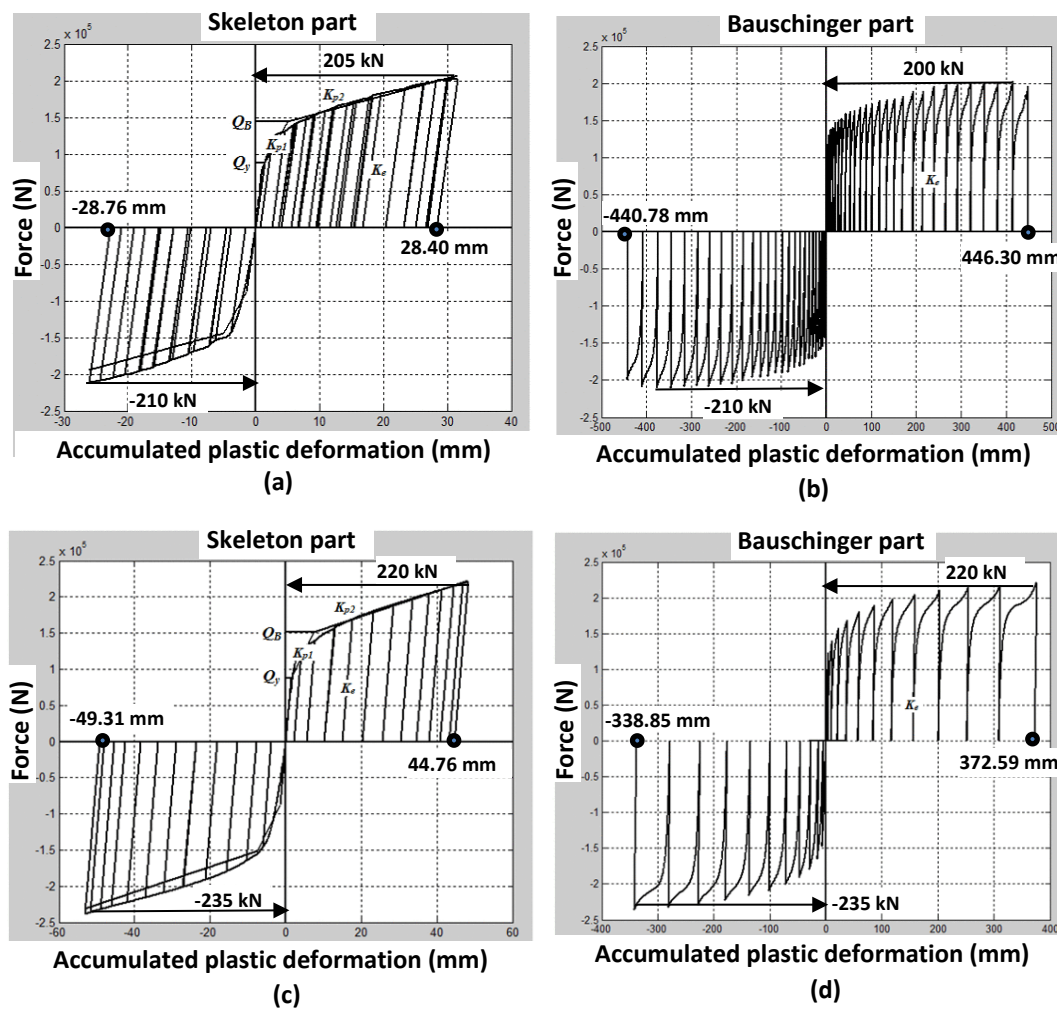


Figure 9. Skeleton parts and Bauschinger parts of the damper due to ATC-24 and $\Phi=2$ ULCF loadings: (a) and (b) skeleton part and Bauschinger part due to ATC-24; (c) and (d) skeleton part and Bauschinger part due to $\Phi=2$.

For the positive and negative domain of loadings, the dissipated strain energy for skeleton part and Bauschinger part (sW_u^+ and BW_u^+ , sW_u^- and BW_u^-) and accumulated plastic deformation for skeleton part and Bauschinger part ($s\delta_u^+$ and $B\delta_u^+$, $s\delta_u^-$ and $B\delta_u^-$) can be quantified following the procedures proposed by Benavent Climent [4]. The quantified items are shown in table 2. The total dissipated strain energy

is the sum of the dissipated strain energy by the skeleton part and the Bauschinger part. Observing the hysteretic curves due to four ULCF loads in figure 8, the damper is proven to be very ductile.

Table 2. Dissipated strain energy and accumulated plastic deformation.

ULCF Loads	Dissipated Energy and Accumulated Plastic Defomation	Skeleton part	Bauschinger part
$\Delta = 24$	Positive domain (${}_S W_u^+$ and ${}_B W_u^+$)	4.86e+06 N.mm	6.53e+07 N.mm
	Negative domain (${}_S W_u^-$ and ${}_B W_u^-$)	-4.07e+06 N.mm	-7.11e+07 N.mm
	Positive domain (${}_S \delta_u^+$ and ${}_B \delta_u^+$)	28.40 mm	446.30 mm
	Negative domain (${}_S \delta_u^-$ and ${}_B \delta_u^-$)	-22.76 mm	-440.78 mm
$\Phi = 2$	Positive domain (${}_S W_u^+$ and ${}_B W_u^+$)	7.99e+06 N.mm	6.20e+07 N.mm
	Negative domain (${}_S W_u^-$ and ${}_B W_u^-$)	-9.60e+06 N.mm	-6.17e+07 N.mm
	Positive domain (${}_S \delta_u^+$ and ${}_B \delta_u^+$)	44.76 mm	372.59 mm
	Negative domain (${}_S \delta_u^-$ and ${}_B \delta_u^-$)	-49.31 mm	-338.85 mm
$\Phi = 10$	Positive domain (${}_S W_u^+$ and ${}_B W_u^+$)	1.30e+07 N.mm	2.27e+07 N.mm
	Negative domain (${}_S W_u^-$ and ${}_B W_u^-$)	-1.14e+07 N.mm	-1.76e+07 N.mm
	Positive domain (${}_S \delta_u^+$ and ${}_B \delta_u^+$)	67.84 mm	131.93 mm
	Negative domain (${}_S \delta_u^-$ and ${}_B \delta_u^-$)	-55.01 mm	-93.56 mm
$\Delta = 30$	Positive domain (${}_S W_u^+$ and ${}_B W_u^+$)	7.84e+06 N.mm	5.66e+07 N.mm
	Negative domain (${}_S W_u^-$ and ${}_B W_u^-$)	-1.55e+07 N.mm	-4.65e+07 N.mm
	Positive domain (${}_S \delta_u^+$ and ${}_B \delta_u^+$)	43.52 mm	299.71 mm
	Negative domain (${}_S \delta_u^-$ and ${}_B \delta_u^-$)	-78.28 mm	-226.67 mm

5. Conclusion

Simulation studies and test results of the combined rings and horizontal steel pipe damper showed that the hysteretic curves of the developed damper are stable and fat. Besides being stable and fat, the hysteretic curves have many plastic cycles under four ULCF loadings, therefore the developed damper qualifies as a high performance damper that can be used to reduce the seismic response of the building significantly due to strong earthquakes. Adopting the appropriate value of c_1 and c_2 , the coefficients for near-fault and far-field earthquakes proposed by Manfredi et al. [5], the dampers can be used as seismic energy dissipating devices for structures located at near-fault or far-field earthquake areas.

Acknowledgment

This research was supported by the Decentralization Research Grant (FTSL PN-1-08-2014 and FTSL PN-1-08-2015) of Directorate General of Higher Education (DIKTI), Ministry of National Education, Indonesia.

References

- [1] Mahjoubi S and Maleki S 2017 *Struct. Control Health Monit.* **24** e1869
- [2] ABAQUS *user's manual, version 6.11* Dassault Systemmes Corp. Providence RI USA
- [3] Kanvinde A M and Deierlein G G 2006 *J. Struct. Eng.* **132** 171–182
- [4] Benavent-Climent A 2007 *Earthq. Eng. Struct. D.* **36** 1049-1064
- [5] Manfredi G, Polese M and Cosenza E 2003 *Earthq. Eng. Struct. D.* **32** 1853-1865